NeuroImage 188 (2019) 70–83

Contents lists available at ScienceDirect

NeuroImage

journal homepage: www.elsevier.com/locate/neuroimage

Tonic thermonociceptive stimulation selectively modulates ongoing neural oscillations in the human posterior insula: Evidence from intracerebral EEG

Giulia Liberati [a,*], Maxime Algoet [a], Susana Ferrao Santos [b], Jose Geraldo Ribeiro-Vaz [c], Christian Raftopoulos [c], André Mouraux [a]

[a] Institute of Neuroscience, Université catholique de Louvain, 1200, Brussels, Belgium
[b] Department of Neurology, Saint-Luc University Hospital, 1200, Brussels, Belgium
[c] Department of Neurosurgery, Saint-Luc University Hospital, 1200, Brussels, Belgium

A B S T R A C T

The human insula is an important target for spinothalamic input, but there is still no consensus on its role in pain perception and nociception. In this study, we show that the human insula exhibits activity preferential for sustained thermonociception. Using intracerebral EEG recorded from the insula of 8 patients (2 females) undergoing a presurgical evaluation of focal epilepsy (53 contacts: 27 anterior, 26 posterior), we "frequency-tagged" the insular activity elicited by sustained thermonociceptive and vibrotactile stimuli, by periodically modulating stimulation intensity at a fixed frequency of 0.2 Hz during 75 s. Both types of stimuli elicited an insular response at the frequency of stimulation (0.2 Hz) and its harmonics, whose magnitude was significantly greater in the posterior insula compared to the anterior insula. Compared to vibrotactile stimulation, thermonociceptive stimulation exerted a markedly greater 0.2 Hz modulation of ongoing theta-band (4–8 Hz) and alpha-band (8–12 Hz) oscillations. These modulations were also more prominent in the posterior insula compared to the anterior insula. The identification of oscillatory activities preferential for thermonociception could lead to new insights into the physiological mechanisms of nociception and pain perception in humans.

1. Introduction

To this date, no brain response was shown to be both necessary and sufficient to generate the experience of pain. Nociceptive responses elicited in the human insula are no exception. Despite being an important target for spinothalamic input, the role of the insula in nociception and pain perception is still debated (Davis et al., 2015; Segerdahl et al., 2015a). It was suggested that only specific subregions of the insula might be selectively involved in the perception of pain. For instance, Craig (Craig, 2003, 2002) argued that pain arises within an interoceptive system involving the posterior insula, together with other distinct feelings that originate from inside the body, such as itch and temperature. Segerdahl at al (Segerdahl et al., 2015b). reported that the dorsal posterior insula tracks the intensity of sustained pain – a finding that is consistent with several tract tracing and microelectrode studies in primates suggesting an important role of this region in the processing of nociceptive input and/or in pain perception (Craig, 2014; Evrard et al., 2014). In contrast, Davis et al. (1998) provided support for a role of the anterior insula, but not of the posterior insula, in the perception of painful stimuli.

Studies conducted using intracerebral EEG have shown that transient thermonociceptive stimuli elicit robust low-frequency phase-locked local field potentials (LFPs) in the human insula (Frot et al., 2014, 2007), but these responses can also be elicited – at the same insular locations – by salient non-nociceptive and non-painful tactile, auditory and visual stimuli (Liberati et al., 2018, 2016). Hence, low-frequency phase-locked LFPs recorded from the human insula appear to reflect multimodal activity largely unspecific for nociception and pain, possibly triggered by any salient stimulus occurring in the environment, regardless of its sensory modality. In addition to low-frequency phase-locked LFPs, thermonociceptive stimuli, but not equally arousing tactile, auditory and visual stimuli, were shown to elicit gamma-band oscillations in both the anterior and posterior insula (Liberati et al., 2018, 2017). However, although insular gamma-band oscillations appear to reflect activity preferential for thermonociception and/or the processing of spinothalamic input, their magnitude can be dissociated from pain perception (Liberati et al., 2018), indicating that a significant portion of these responses is not directly related to the quality and intensity of the corresponding sensation.

A drawback of many studies investigating nociception and pain perception in humans is that they rely on responses to very brief thermonociceptive stimuli, generally lasting only a few milliseconds. Such stimuli activate almost exclusively quickly-adapting mechano-heat nociceptors. In contrast, long-lasting thermonociceptive stimuli also generate sustained activity in slowly-adapting thermonociceptors.

* Corresponding author. Avenue Mounier 53, 1200, Brussels, Belgium.
E-mail address: giulia.liberati@uclouvain.be (G. Liberati).

https://doi.org/10.1016/j.neuroimage.2018.11.059
Received 29 August 2018; Received in revised form 15 November 2018; Accepted 30 November 2018
Available online 5 December 2018

Hence, the processes underlying the perception of transient pain and sustained pain could be very different (Meyer and Campbell, 1981; Schepers and Ringkamp, 2010; Treede et al., 1995). To gain a better understanding of the cortical representation of ongoing pain, it is therefore desirable to shift towards novel experimental approaches that can characterize cortical activity induced by sustained thermonociceptive stimulation.

Here, we acquired intracerebral EEG data from the insula of eight epileptic patients, to characterize insular activity related to the perception of sustained heat pain, and to assess its selectivity by comparing it to the activity generated by sustained vibrotaction. Participants were exposed to sustained thermonociceptive and non-nociceptive vibrotactile stimulation, whose intensity was periodically modulated at a constant frequency of 0.2 Hz. Previous scalp EEG studies have shown that sustained periodic sensory stimulation elicits an enhancement of EEG power at the frequency of stimulation and its harmonics (Colon et al., 2016; Mouraux et al., 2011; Nozaradan et al., 2017), and may induce a periodic modulation of ongoing EEG oscillations occurring in different frequency bands (Colon et al., 2016). Furthermore, the perception of sustained pain has been suggested to relate to sustained changes in the magnitude of ongoing EEG oscillations within different frequency bands (Colon et al., 2016; Giehl et al., 2014; Huishi Zhang et al., 2016; Schulz et al., 2015). Given the lack of consensus on the differential role of the posterior and anterior human insula in the processing of nociceptive stimuli, we also investigated whether these differ in their responses to the two types of stimulation.

2. Materials and methods

2.1. Participants

Eight patients (2 females; age: 37 ± 9 years, mean ± standard deviation) suffering from intractable focal epilepsy were recruited over 1 year at the Department of Neurology of the Saint Luc University Hospital (Brussels, Belgium). All patients were investigated using depth electrodes implanted in various brain regions suspected to be the origins of seizures, including wide portions of the anterior and posterior insula (Fig. 1; see Table 1 for the MNI coordinates of each electrode contact). The intracerebral EEG was recorded from 13 depth electrodes located in the insula (Patients 1, 3, 5, 7, and 8 were respectively implanted with two distinct insular electrodes). Five patients were implanted in the left insula (34 contacts), and three patients were implanted in the right insula (19 contacts), for a total of 53 insular contacts (27 contacts in the anterior insula, 26 contacts in the posterior insula). The anterior insula was identified as the region encompassing the short insular gyri (anterior, middle, and posterior), the pole of the insula, and the transverse insular gyrus. The posterior insula was identified as the region encompassing the anterior and posterior long insular gyri (Naidich et al., 2004). The anonymized DICOM images of each patient are available at the OSF online repository at the address https://osf.io/zj6rv/. These images do not include facial features that could lead to the identification of the participants.

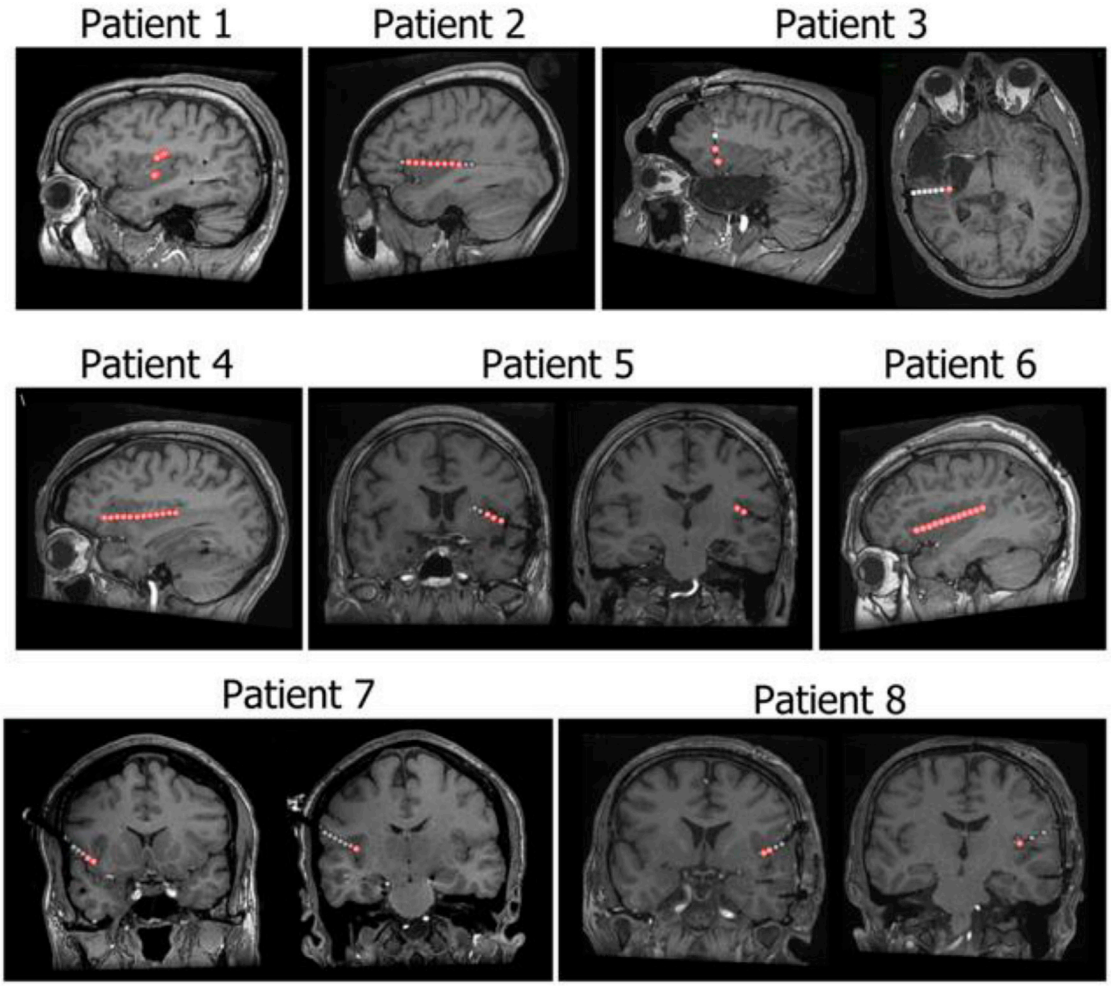

Fig. 1. Localization of the 13 depth electrodes implanted in the insula of 8 patients. A total of 53 insular sites (27 in the anterior insula, 26 in the posterior insula; 34 in the left insula, 19 in the right insula; indicated by red circles) were investigated. The MNI coordinates of the electrode contacts are presented in Table 1. The DICOM images of each patient are available at the OSF online repository at the address https://osf.io/zj6rv/.

Table 1
Localization of insular electrode contacts.

Subject	Hemisphere	Contact	Description	MNI coordinates
1 (electrode 1)	Left	1	Posterior insular cortex, external capsule	−33, −12, 13
		2	Posterior insular cortex, transition between the long gyrus of the insula and the cortex from the parietal operculum, at the level of the circular gyrus	−38, −12, 14
		3	Posterior insular cortex, transition between the long gyrus of the insula and the cortex from the parietal operculum, at the level of the circular gyrus	−44, −12, 17
		4	Posterior insular cortex/parietal operculum	−49, −12, 16
1 (electrode 2)	Left	1	Posterior insular cortex, most posterior long gyrus	−38, −9, −5
		2	Posterior insular cortex, most posterior long gyrus	−42, −9, −5
2	Left	1	Anterior insular cortex, adjacent to the opercular portion of the inferior frontal gyrus	−42, 22, −1
		2	Anterior insular cortex, adjacent to the opercular portion of the inferior frontal gyrus	−42, 16, −1
		3	Anterior insular cortex, second short gyrus	−42, 11, −1
		4	Anterior insular cortex, transition between the second and third short gyri	−42, 4, −1
		5	Anterior insular cortex, third short gyrus	−42, −1, 0
		6	Posterior insular cortex, first long gyrus	−42, −8, 0
		7	Posterior insular cortex, transition between the first long gyrus and the second long gyrus	−42, −15, 0
		8	Posterior insular cortex, second long gyrus	−42, −19, 0
3 (electrode 1)	Right	1	Anterior insular cortex, first short gyrus	37, 22, −11
		2	Anterior insular cortex, first short gyrus adjacent to the inferior frontal gyrus	37, 27, 0
3 (electrode 2)	Right	1	Posterior insular cortex, ventral portion of the second long gyrus	35, −17, 7
4	Left	1	Anterior insular cortex, adjacent to the inferior frontal gyrus	−33, 29, −9
		2	Anterior insular cortex, adjacent to the inferior frontal gyrus	−33, 24, −8
		3	Anterior insular cortex, adjacent to the inferior frontal gyrus	−34, 19, −7
		4	Anterior insular cortex, first short gyrus	−34, 14, −6
		5	Anterior insular cortex, second short gyrus	−34, 9, −3
		6	Anterior insular cortex, transition between the second and third short gyri	−35, 3, −2
		7	Anterior insular cortex, third short gyrus	−35, −2, 0
		8	Anterior insular cortex, transition between the third short gyrus and the first long gyrus	−35, −6, 3
		9	Posterior insular cortex, first long gyrus	−35, −11, −5
		10	Posterior insular cortex, first long gyrus	−35, −16, 6
		11	Posterior insular cortex, transition between the first long gyrus and the second long gyrus	−35, −21, 8
		12	Posterior insular cortex, transition between the first long gyrus and the second long gyrus	−35, −26, 11
5 (electrode 1)	Left	1	Anterior insular cortex, first short gyrus	−35, 14, −1
		2	Anterior insular cortex, adjacent to the opercular portion of the inferior frontal gyrus	−39, 14, −3
		3	Anterior insular cortex, adjacent to the opercular portion of the inferior frontal gyrus	−44, 13, −6
5 (electrode 2)	Left	1	Posterior insular cortex, dorsal portion of the first long gyrus	−40, −11, 12
		2	Posterior insular cortex, dorsal portion of the first long gyrus	−44, −11, 9
6	Right	1	Anterior insular cortex, adjacent to the inferior frontal gyrus	40, 23, −6
		2	Anterior insular cortex, transition between the first short gyrus and the second short gyrus	40, 19, −4
		3	Anterior insular cortex, second short gyrus	40, 13, −2
		4	Anterior insular cortex, second short gyrus	40, 9, 0
		5	Anterior insular cortex, third short gyrus	40, 4, 1
		6	Anterior insular cortex, third short gyrus	40, 0, 3
		7	Anterior insular cortex, third short gyrus	40, −5, 5
		8	Posterior insular cortex, first long gyrus	40, −10, 7
		9	Posterior insular cortex, first long gyrus	40, −15, 9
		10	Posterior insular cortex, first long gyrus, adjacent to the transverse temporal gyrus	40, −20, 11
		11	Posterior insular cortex, transition between the first long gyrus and the second long gyrus, adjacent to the transverse temporal gyrus	40, −24, 12
		12	Posterior insular cortex, second long gyrus, adjacent to the transverse temporal gyrus	40, −30, 15
7 (electrode 1)	Right	1	Anterior insular cortex, adjacent to the opercular portion of the inferior frontal gyrus	44, 15, −9
7 (electrode 2)	Right	1	Posterior insular cortex, dorsal portion of the second long gyrus	44, −12, 8
		2	Posterior insular cortex, dorsal portion of the first long gyrus	48, −12, 11
		3	Posterior insular cortex/operculus	52, −12, 14
8 (electrode 1)	Left	1	Anterior insular cortex, second short gyrus	−40, 9, −4
		2	Anterior insular cortex, second short gyrus, adjacent to the frontal operculum cortex	−44, 9, −2
8 (electrode 2)	Left	1	Posterior insular cortex, first long gyrus	−39, −11, 8

None of the participants had psychiatric issues, cognitive impairment, or sensory abnormalities. None of the participants presented ictal discharge onset in the insula during the recordings, and low-voltage fast activity was never present in the insula during spontaneous seizures. Four of the patients (Patients 1, 2, 4 and 5) also participated in other studies conducted by our team (Liberati et al., 2017, 2016). All experimental procedures were approved by the local Research Ethics Committee (Commission Ethique de l'Université catholique de Louvain, B403201316436). The manuscript does not contain information or images that could lead to the identification of the participants.

2.2. Experimental design

The study was conducted at the patient bedside. Before the beginning of the experiment, patients were briefly exposed to the test stimuli for familiarization. The experiment consisted of two blocks, which were randomized across participants (Fig. 2). The two blocks were either delivered on the same day or on two different days, according to each patient's health condition and availability. In one block, participants received sustained periodic thermonociceptive stimuli. In the other block, participants received sustained periodic non-nociceptive

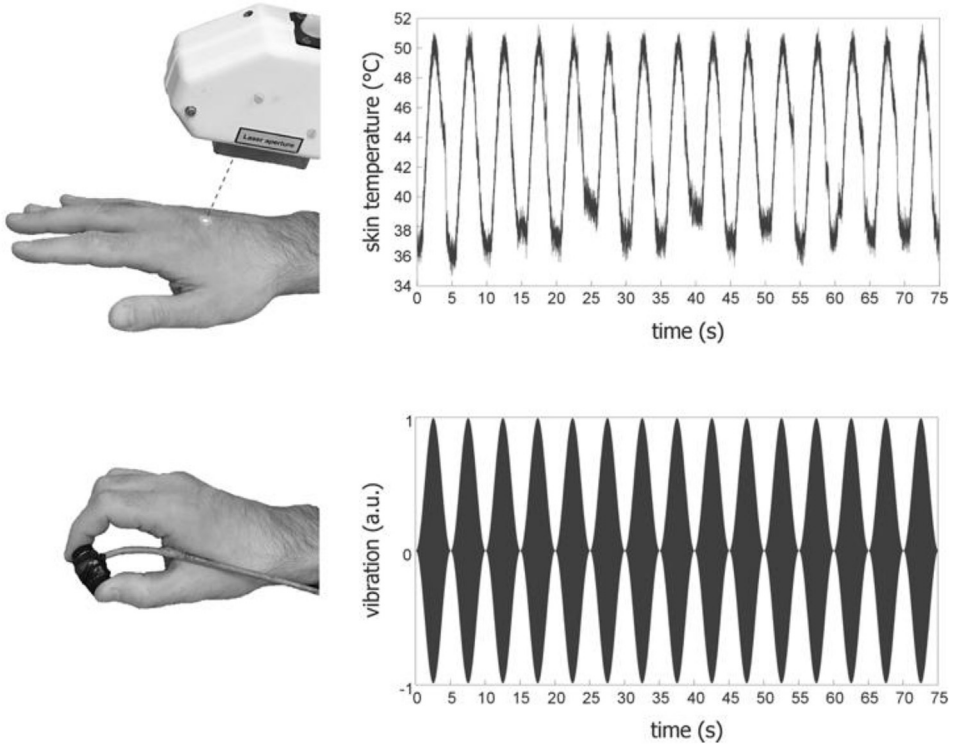

Fig. 2. Experimental procedure. The experiment consisted of two blocks of sustained periodic stimulation (thermonociceptive, upper panel; and vibrotactile, lower panel), randomized across participants. *Sustained periodic thermonociceptive stimuli*, delivered on the hand dorsum contralateral to the implanted insular electrodes, were generated using a temperature-controlled CO_2 laser stimulator. The power output of the laser stimulator was regulated online using a feedback control loop based on a continuous measurement of the skin temperature at the site of stimulation. The stimuli consisted in a 0.2 Hz sinusoidal variation of skin temperature, oscillating between baseline skin temperature and 50 °C, for a duration of 75 s (15 cycles, each lasting 5 s; one representative stimulus shown). *Sustained periodic vibrotactile stimuli* were delivered via a recoil-type vibrotactile transducer driven by a standard audio amplifier, positioned between the fingertips of the index and the thumb contralateral to the implanted insular electrode. The vibrations had a mean frequency of 251 Hz. Such as for thermonociceptive stimulation, the amplitude was periodically modulated at a frequency of 0.2 Hz (15 cycles, each lasting 5 s, for a total of 75 s; a.u., arbitrary amplitude unit).

vibrotactile stimuli, matching the thermonociceptive stimuli in frequency and duration. The order of the blocks was randomized across participants. At the end of each block, participants were asked to describe the quality of perception, and to report whether they had perceived the stimuli as painful.

Sustained periodic thermonociceptive stimuli, delivered on the hand dorsum contralateral to the implanted insular electrodes, were generated using a temperature-controlled CO_2 laser stimulator (Laser Stimulation Device, SIFEC, Belgium). The power output of this stimulator is regulated online using a feedback control loop based on a continuous measurement of the skin temperature at the site of stimulation, performed using a radiometer collinear with the laser beam. Because this radiometer allows obtaining a reliable estimate of target temperature with a very short integration time, the feedback loop is capable of updating laser power output at a very fast rate (500 Hz). The heat source is a 25 W radiofrequency-excited CO_2 laser (Synrad 48-2; Synead, WA). Power control is achieved by pulse width modulation at a 5-kHz clock frequency. The stimuli are delivered through a 6 m optical fiber. By vibrating this fiber at some distance of the source, a quasi-uniform spatial distribution of radiative power within the stimulated area is obtained. At the end of the fiber, optics are used to collimate the beam. In this experiment, the optics provided a 12-mm beam diameter at target site. The thermonociceptive stimuli consisted in a 0.2 Hz sinusoidal variation of skin temperature, oscillating between baseline skin temperature (33 ± 3 °C; mean ± standard deviation) and 50 °C (except for Patient 7 who received thermonociceptive stimulation at the maximal temperature of 48 °C, as the stimulation at 50 °C was perceived as too painful). The 50 °C temperature was chosen because it is above the thermal activation threshold of both slowly- and quickly-adapting thermonociceptors (Dubin and Patapoutian, 2010). The decision to use a frequency of stimulation of 0.2 Hz was driven by the results of our previous scalp EEG study, in which we found that modulating the intensity of a sustained heat stimulus at 0.2 Hz elicits a periodic EEG response having a high signal-to-noise ratio, enabling the identification of clear peaks in the frequency spectrum – at the frequency of stimulation and at its harmonics – at single subject level (Colon et al., 2016). Previous microneurography studies indicate that sustained heat stimuli modulated at 0.2 Hz should elicit strong activity in slowly-adapting C-fiber nociceptors, which are thought to play an important role in the perception of tonic heat pain (Meyer and Campbell, 1981; Treede et al., 1995). Another advantage of using this low frequency of modulation is that is allows exploring the modulation of ongoing EEG rhythms down to the range of theta-band oscillations.

The duration of the sustained periodic thermonociceptive stimulus was 75 s (15 cycles, each lasting 5 s). To avoid sensitization or habituation of heat-sensitive afferents, the target of the laser beam on the skin was slightly displaced during the descending part of each stimulation cycle. In a previous behavioral experiment, in which we asked participants to continuously evaluate the intensity of this type of stimulus by manipulating a slider, we showed that subjects perceived a sustained sensation of burning heat, whose intensity increased and decreased periodically over time. (Colon et al., 2016). We delivered up to 20 sustained periodic thermonociceptive stimuli for each participant. Given the duration of stimulation, patients could interrupt the block at any time if they were too tired. Therefore, 14 ± 4 (mean ± standard deviation) thermonociceptive stimuli were delivered.

Sustained periodic vibrotactile stimuli were delivered via a recoil-type vibrotactile transducer driven by a standard audio amplifier (Haptuator, Tactile Labs Inc., Canada), positioned between the fingertips of the index and the thumb contralateral to the implanted insular electrode. The vibrations had a mean frequency of 251 Hz. This type of stimulation was chosen because, despite being non-painful, it is perceived as highly intense. Such as for thermonociceptive stimulation, its amplitude was periodically modulated at a frequency of 0.2 Hz (15 cycles, each lasting 5 s, for a total of 75 s). The vibrotactile block could be interrupted at any time if the patient was too tired. Therefore, 16 ± 2 (mean ± standard deviation) vibrotactile stimuli were delivered.

2.3. Intracerebral recordings and anatomical electrode contact localization

For each patient, a tailored implantation strategy was planned according to the regions considered most likely to be ictal onset sites or

propagation sites, as described in previous work from our group (Liberati et al., 2017, 2016). Target areas, including the insular cortex, were reached using commercially available depth electrodes (AdTech, Racine, WI, U.S.A.; electrode rod diameter: 1.1 mm; contact length: 2.4 mm; contact spacing: 5 mm), implanted using a frameless stereotactic technique through burr holes. The placement of the electrodes was guided by a neuronavigation system based on 3D-T1w magnetic resonance (MRI) sequence performed in a 1.5 T scanner (Gradient Echo; flip angle: 15°; TR: 7.5 s; TE minimum full; 3.1–13 ms; slice thickness: 1 mm; FOV: 24 cm; matrix: 224 × 224; number of slices: 162). A post-implantation 3D-T1 MRI sequence, performed either right after the surgery or on the following day, was used to accurately identify the locations of each electrode contact. This acquisition mode is safe and compatible with implanted electrodes. To obtain the MNI coordinates of each insular electrode contact, individual MRI scans were normalized to a standard T1 template in MNI space using Brain Voyager 20.2 (Brain Innovation, Maastricht, The Netherlands). The MNI coordinates were further used to generate group-level 3D glass brain plots of response amplitude at each contact location in the left and right insula, such as to visualize their spatial distributions. These plots were generated using the iELVis open source Matlab toolbox (Groppe et al., 2017) and a FreeSurfer anatomical atlas (http://surfer.nmr.mgh.harvard.edu/), after performing nonlinear mapping between the MNI volumetric coordinate system and the FreeSurfer surface coordinate system (Wu et al., 2018).

The intracerebral EEG recordings were performed using a DeltaMed (Paris, France) acquisition system. Additional bipolar channels were used to record electromyographic activity (EMG: two electrodes measuring respectively bicipital and tricipital contraction of the patient's non-dominant arm) and electrocardiographic activity (EKG: two channels, utilizing two electrodes respectively located on the right and left side of the sternum, one electrode located centrally under the sternum, and one electrode on the right lateral side of the chest). All signals were acquired at a 512 Hz sampling rate using a reference electrode located between Cz and Pz, re-referenced to the average activity recorded from all intracerebral contacts, and analyzed offline using Letswave 6 (https://github.com/NOCIONS/letswave6) (Mouraux and Iannetti, 2008). The continuous intracerebral EEG recordings were filtered using a 0.05 Hz high-pass Butterworth filter to remove slow drifts in the recorded signals. Non-overlapping epochs were obtained by segmenting the recordings from 0 to 75 s relative to the onset of each sustained periodic stimulation. Artifacts due to eye blinks, eye movements, or muscular activity were removed using a validated method based on an Independent Component Analysis (FastICA algorithm) (Hyvärinen and Oja, 2000). Epochs containing excessive artifacts that could not be removed using FastICA were rejected from further analyses using visual inspection. 2 ± 3 (mean ± standard deviation) epochs were rejected in the thermonociceptive blocks, and 3 ± 2 (mean ± standard deviation) epochs were rejected in the vibrotactile blocks.

2.4. Statistical analyses

For each patient and modality of stimulation, the artifact-free intracerebral EEG epochs were averaged. The obtained average waveforms, lasting 75 s, were then transformed in the frequency domain using a discrete Fourier transform (FFTW) (Frigo and Johnson, 1998). We then used a "frequency-tagging" (Regan, 1989) approach to identify the responses to the sustained periodic thermonociceptive and vibrotactile simulations. The general assumption underlying this frequency-domain analysis approach is that sustained periodic stimulation elicits periodic activity within the neurons processing this input, and that this synchronous neuronal activity generates peaks in the EEG frequency spectrum at the frequency of stimulation and its harmonics (Colon et al., 2016, 2014; 2012b, 2012a; Mouraux et al., 2011). Therefore, at these frequencies, the amplitude of the FFTW may be expected to correspond to the sum of the stimulus-evoked periodic intracerebral EEG response and unrelated residual background noise that was not completely canceled out by the averaging procedure. To obtain valid estimates of the magnitude of the periodic intracerebral EEG responses, we thus removed the contribution of this residual noise by subtracting, at each insular contact and at each frequency bin, the average amplitude of the signal measured at neighboring frequencies (−0.026 to −0.065 Hz and +0.026 to +0.065 Hz) (Colon et al., 2016; Mouraux et al., 2011). In the absence of a periodic intracerebral EEG response, the noise-subtracted average signal amplitude is expected to tend toward zero. Therefore, to assess the significance of the periodic responses, a non-parametric Wilcoxon signed-rank test was used to determine whether, for each modality of stimulation (thermonociceptive and vibrotactile), the magnitude of the noise-subtracted signal amplitude at the base frequency (0.2 Hz) and at the harmonic frequencies (0.4 Hz, 0.6 Hz, and 0.8 Hz), averaged across all insular contacts, were significantly greater than zero. Significance level was set at $p < .05$, uncorrected for multiple comparisons.

Comparison of the periodic intracerebral EEG responses elicited by sustained thermonociceptive and vibrotactile stimulation in the anterior and posterior insula was conducted using IBM SPSS Statistics 24 (Armonk, NY). A linear mixed models (LMM) analysis with 'modality' (two levels: thermonociceptive, vibrotactile), 'harmonic frequency' (three levels: 0.2 Hz, 0.4 Hz, 0.6 Hz; corresponding to the harmonic frequencies at which the noise-subtracted amplitudes were significantly greater than zero), and 'location' (2 levels: average signal at anterior insula contacts, and posterior insula contacts) as fixed factors was used. Given the high discrepancy in the number of electrode contacts located in the right and left insulae, the factor 'side' was not included. To account for the variation of the regression model intercept across participants, the contextual variable 'subject'. was added to the LMM. Parameters were estimated using restricted maximum likelihood (REML) (Twisk, 2005). Main effects were compared using the Bonferroni confidence interval adjustment.

Time course of periodic insular activity. To assess the time course of periodic insular responses over the 75 s of sustained periodic stimulation, we computed an additional set of epochs by segmenting the 75 s waveforms into three successive segments of 25 s (0–25 s, 25–50 s, 50–75 s), and processed the data as in the previous analyses. To obtain valid estimates of the magnitude of the periodic intracerebral EEG responses, we removed the contribution of this residual noise by subtracting, at each insular contact and at each frequency bin, the average amplitude of the signal measured at neighboring frequencies (−0.08 to −0.2 Hz and +0.08 to +0.2 Hz).

For each modality, we then performed a LMM analysis on the noise-subtracted signal amplitude at 0.2 Hz using 'segment' (three levels: first, second, third) and 'harmonic frequency' (three levels: 0.2 Hz, 0.4 Hz, 0.6 Hz) as fixed factors, and 'subject' as a contextual variable. Parameters were estimated using REML (Twisk, 2005).

Hilbert analysis. To examine whether sustained periodic thermonociceptive stimulation and/or sustained periodic vibrotactile stimulation generated a periodic modulation of the amplitude of ongoing intracerebral EEG oscillations within different frequency bands of the EEG frequency spectrum, band-pass Butterworth filters were applied to the unaveraged EEG epochs to retain the EEG signal within theta (4–8 Hz), alpha (8–12 Hz), beta (12–40 Hz), and gamma (40–100 Hz) frequency bands. A Hilbert transform was then applied to the filtered EEG epochs to estimate the envelope of the signal within each frequency band. Finally, the obtained epochs were averaged across trials, transformed in the frequency domain using a FFTW, and noise subtracted using the mean of the signal amplitude measured at neighboring frequencies (−0.026 to −0.065 Hz and +0.026 to +0.065 Hz). To assess the significance of the periodic modulations of ongoing oscillations, a non-parametric Wilcoxon signed-rank test was used to determine whether, for each modality of stimulation and frequency band, the magnitudes of the noise-subtracted modulations at the base frequency (0.2 Hz) and at the harmonic frequencies (0.4 Hz, 0.6 Hz, and 0.8 Hz), averaged across all insular contacts, were significantly greater than zero. Significance level was set at $p < .05$, uncorrected for multiple comparisons.

We then performed a LMM analysis with 'modality' (two levels: thermonociceptive, vibrotactile), 'frequency band' (theta, alpha, beta, gamma), 'harmonic frequency' (four levels: 0.2 Hz, 0.4 Hz, 0.6 Hz, 0.8 Hz; corresponding to the harmonic frequencies at which the noise-subtracted amplitudes were significantly greater than zero), and 'location' (two levels: anterior insula and posterior insula) as fixed factors and 'subject' as a contextual variable. Parameters were estimated using REML (Twisk, 2005).

3. Results

3.1. Quality of perception

All participants described the sensation elicited by the sustained periodic thermonociceptive stimuli as a diffuse mildly painful sensation of heat, with the exception of Patient 7, who described the stimulation as intensely burning (for this reason, the block was interrupted after 6 trials). All participants described the sensation elicited by the sustained periodic vibrotactile stimuli as not painful, but nevertheless intense.

3.2. Periodic insular signals elicited by thermonociceptive and vibrotactile stimulation

Both thermonociceptive and vibrotactile stimulation elicited a marked increase of EEG power at the frequency corresponding to the frequency of stimulation (0.2 Hz), and at its harmonics (Fig. 3). The Wilcoxon signed-rank test showed that for both modalities, the magnitude of the noise-subtracted signal amplitude averaged across all insular contacts was significantly different from zero at 0.2 Hz, 0.4 Hz, and 0.6 Hz, but not at 0.8 Hz (Table 2; Fig. 4). The LMM analysis performed using 'modality' (thermonociceptive, vibrotactile), 'location' (anterior insula, posterior insula), and 'harmonic frequency' (0.2 Hz, 0.4 Hz, 0.6 Hz) showed a significant interaction between the factors 'location' and 'harmonic frequency' ($F = 24.4$, $p < .001$). Post-hoc comparisons showed that the signal amplitudes at 0.2 Hz and at 0.4 Hz were significantly greater in the posterior insula compared to the anterior insula ($p < .001$ and $p = .001$, respectively). The differences between the 0.2 Hz periodic responses recorded from the anterior and posterior insula for both the thermonociceptive and the vibrotactile modalities are shown in Fig. 5. There was, however, no significant effect of 'modality' ($F = 0.01$, $p = .893$), and no interaction between 'modality' and the other factors, indicating that this feature of the periodic EEG response elicited by sustained thermonociceptive stimulation was largely similar to the periodic EEG response elicited by vibrotactile stimulation.

Table 2
Results of the Wilcoxon signed-rank test used to determine whether, for the thermonociceptive modality and the vibortactile modality, the magnitude of the noise-subtracted signal amplitude at the frequency of stimulation (0.2 Hz) and at the harmonic frequencies was significantly greater than zero.

modality	harmonic frequency	p-value
thermonociceptive	0.2 Hz	**p < .001**
	0.4 Hz	**p < .001**
	0.6 Hz	**p = .004**
	0.8 Hz	p = .774
vibrotactile	0.2 Hz	**p < .001**
	0.4 Hz	**p < .001**
	0.6 Hz	**p = .006**
	0.8 Hz	p = .550

3.3. Temporal dynamics of the periodic insular responses

The LMM analysis of the noise-subtracted signal amplitude within the first (0–25 s), second (25–50 s), and third (50–75 s) segments of each 75-s epoch showed no effect of 'segment', neither for the periodic response elicited by thermonociceptive stimulation ($F = 1.4$, $p = .246$) nor the periodic response elicited by vibrotactile stimulation ($F = 0.2$, $p = .782$). Furthermore, there was no significant interaction between the factors 'segment' and 'harmonic frequency', indicating that the magnitude of the periodic responses at 0.2 Hz, 0.4 Hz, and 0.6 Hz all tended to remain constant over time, both for thermonociceptive ($F = 1.1$, $p = .379$) and vibrotactile ($F = 0.4$, $p = .252$) stimulation (Fig. 6).

3.4. Periodic modulation of ongoing oscillations (Hilbert analysis)

The results of the Wilcoxon signed-rank test to assess the significance of the modulation of ongoing oscillations exerted by thermonociceptive and vibrotactile stimuli in the different frequency bands are shown in

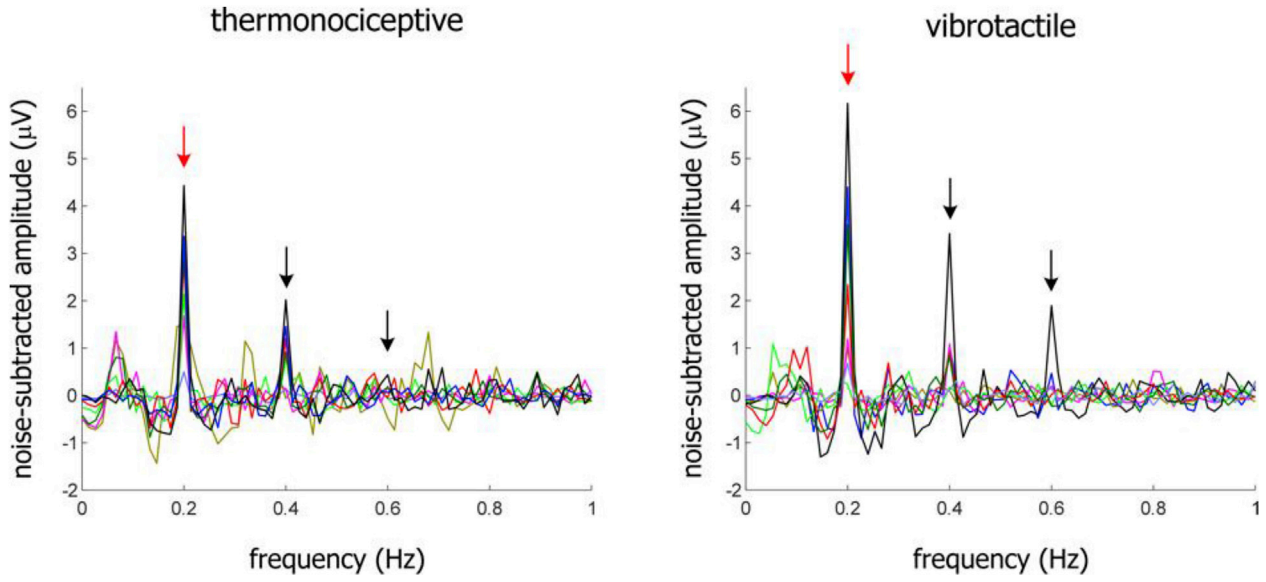

Fig. 3. Frequency-domain analysis of the periodic insular EEG response elicited by 0.2 Hz periodic thermonociceptive and vibrotactile stimulation. Frequency spectrum of the noise-subtracted intracerebral EEG signal measured from the insula of each patient, at the individual insular contact showing the response with the highest amplitude. Note the clear enhancement of amplitude at 0.2 Hz (red arrows) and its harmonics (black arrows), present both during sustained periodic thermonociceptive stimulation (left) and during sustained periodic vibrotactile stimulation (right).

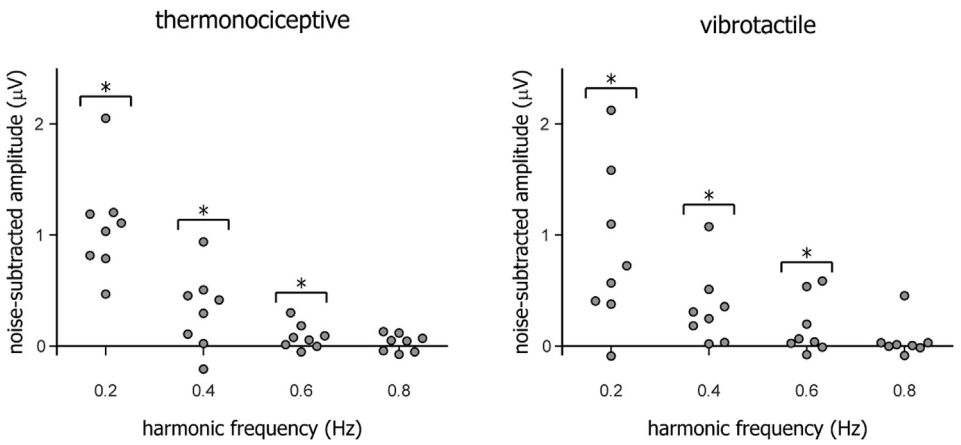

Fig. 4. Individual noise-subtracted amplitude of the insular EEG response elicited at the base frequency (0.2 Hz) and harmonic frequencies (0.4 Hz, 0.6 Hz, 0.8 Hz), averaged for each patient across all insular contacts. Both during thermonociceptive and vibrotactile stimulation, the magnitude of the noise-subtracted signal amplitude was significantly greater than zero at 0.2 Hz, 0.4 Hz and 0.6 Hz, but not at 0.8 Hz *p < .05 (Wilcoxon signed ranked test against zero).

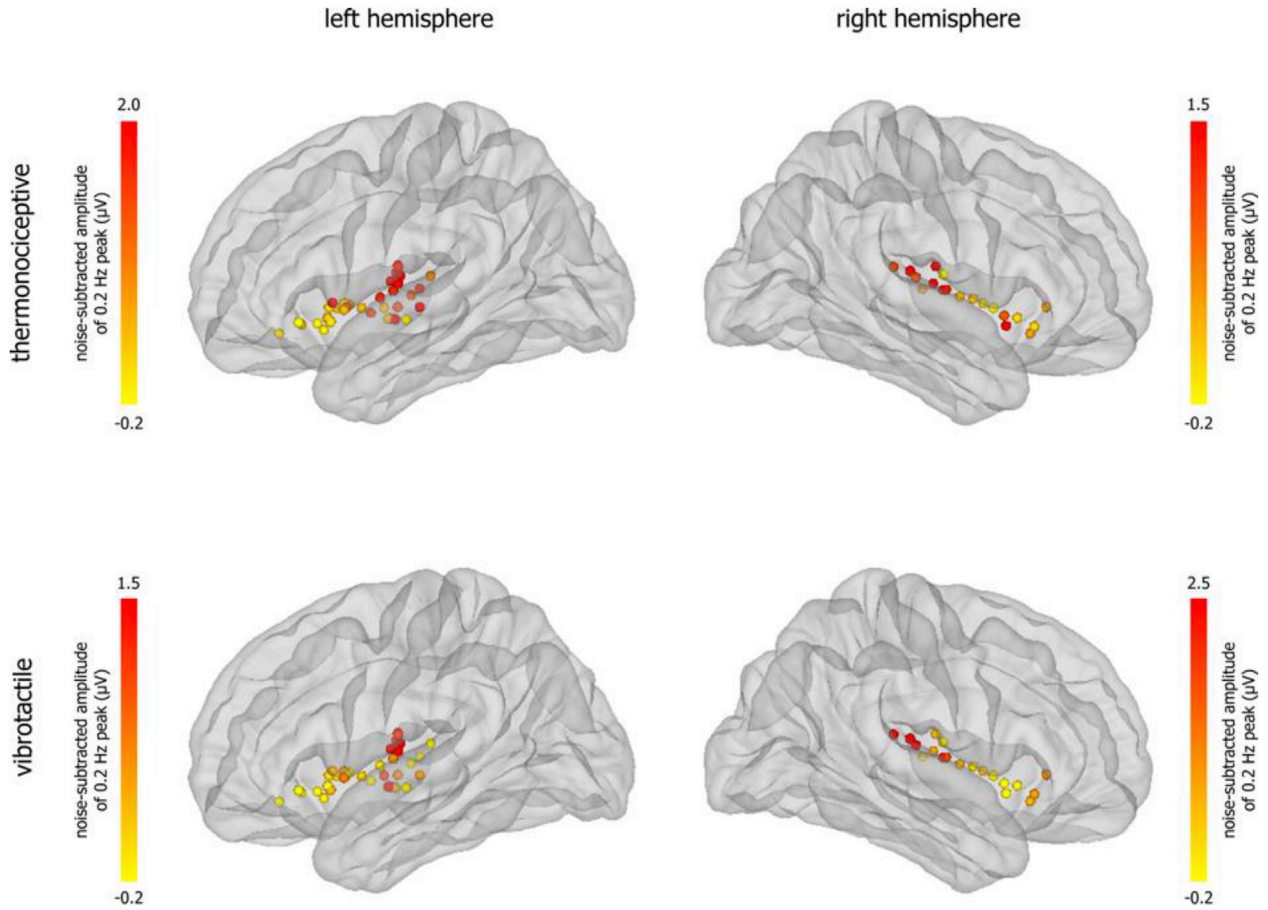

Fig. 5. Spatial distribution of the amplitude of the 0.2 Hz periodic response elicited by thermonociceptive and vibrotactile stimulation. The circles correspond to the MNI coordinates of the insular contacts of all patients, within a 3D glass brain generated using the FreeSurfer template (http://surfer.nmr.mgh.harvard.edu/). Note that, for both modalities of stimulation, the magnitude of the sustained periodic 0.2 Hz response was markedly greater at dorsal-posterior electrode contacts.

Table 3. Thermonociceptive stimulation exerted a highly significant 0.2 Hz modulation of ongoing insular oscillations in the theta, alpha, beta, and gamma frequency bands. In contrast, vibrotactile stimulation did not exert a significant 0.2 Hz modulation in any of the frequency bands (Fig. 7). The LMM analysis performed using 'modality' (thermonociceptive, vibrotactile), 'location' (anterior insula, posterior insula), 'frequency band' (theta, alpha, beta, gamma), and 'harmonic frequency' (0.2 Hz, 0.4 Hz, 0.6 Hz, 0.8 Hz) as factors showed a significant three-way interaction between the factors 'modality', 'frequency band' and 'harmonic frequency' ($F = 5.5$, $p < .001$). Post-hoc comparisons showed that, compared to vibrotactile stimuli, thermonociceptive stimuli elicited a greater modulation of ongoing oscillations at 0.2 Hz and at 0.4 Hz in the theta frequency band (both $p < .001$), and a greater modulation of ongoing oscillations at 0.2 Hz in the alpha frequency band ($p = .002$)

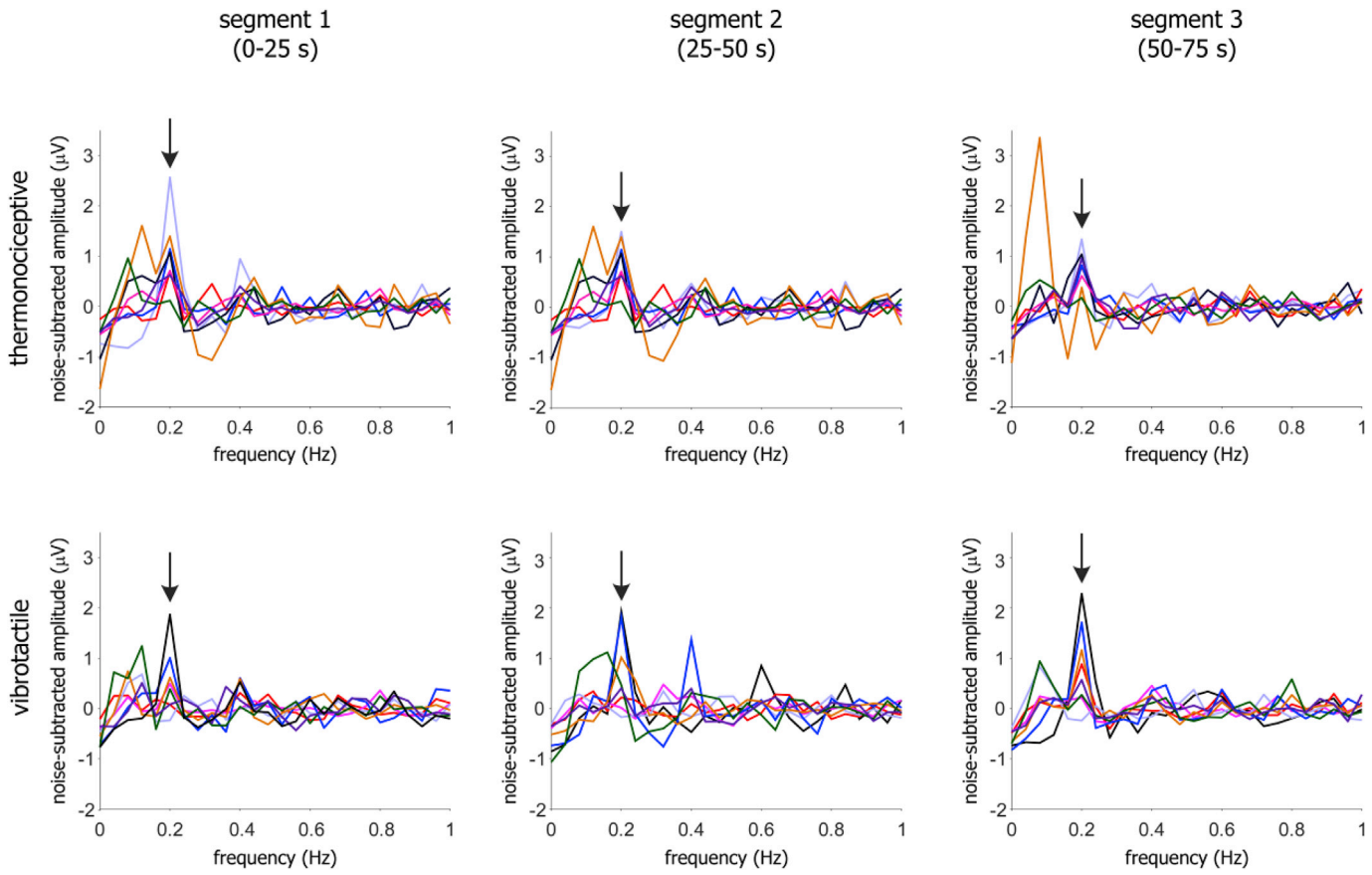

Fig. 6. Temporal dynamics of the periodic insular responses. Amplitude of the 0.2 Hz periodic response elicited by the periodic 0.2 Hz thermonociceptive and vibrotactile stimulation did not differ significantly across the first (0–25 s), second (25–50 s), and third (50–75 s) segments of stimulation, indicating that the elicited activity sustains over time. Each line shows the response of one individual participant, averaged across insular contacts.

Table 3
Results of the Wilcoxon signed-rank test used to determine, whether, for the thermonociceptive modality and the vibrotactile modality, the magnitude of the noise-subtracted modulation of ongoing oscillations within different frequency bands at the frequency of stimulation (0.2 Hz) and at the harmonic frequencies was significantly greater than zero.

harmonic frequency	thermoniceptive stimulation			
	frequency band			
	theta	alpha	beta	gamma
0.2 Hz	**p < .001**	**p < .001**	**p = .001**	**p < .001**
0.4 Hz	p = .001	p = .031	p = .001	p = .082
0.6 Hz	p = .068	p = .707	p = .428	p = .664
0.8 Hz	p = .947	p = .298	**p = .015**	**p = .048**
harmonic frequency	vibrotactile stimulation			
	frequency band			
	theta	alpha	beta	gamma
0.2 Hz	p = .330	p = .933	p = .085	p = .078
0.4 Hz	p = .763	p = .248	**p < .001**	p = .951
0.6 Hz	p = .236	**p = .017**	p = .190	p = .059
0.8 Hz	p = .954	p = .210	**p = .044**	p = .479

(Fig. 8). In addition, the analysis yielded a significant three-way interaction between the factors 'location', 'frequency band', and 'harmonic frequency' (F = 2.9, p = .002). Post-hoc comparisons showed that, in the theta frequency band, the modulation of ongoing oscillations at 0.2 Hz and at 0.4 Hz was significantly greater in the posterior insula compared to the anterior insula (p < .001 and p = .001, respectively); and that in the alpha and beta frequency bands, the modulation of ongoing oscillations at 0.2 Hz was also significantly greater in the posterior insula compared to the anterior insula (p = .019 and p = .007, respectively). The differences in the 0.2 Hz modulations of ongoing theta- and alpha-band oscillations elicited in the anterior and posterior insula by thermonociceptive stimuli are shown in Fig. 9.

4. Discussion

Sustained thermonociceptive stimulation periodically modulated at 0.2 Hz elicited a significant periodic signal in the intracerebral EEG signals recorded from the human insula, appearing as peaks in the EEG frequency spectrum at the frequency of stimulation (0.2 Hz) and its harmonics (0.4 Hz, 0.6 Hz). This periodic signal likely reflects synchronized activity within neuronal populations of the insula responding to the thermonociceptive stimulus (Herrmann, 2001; Nozaradan, 2014). Using scalp EEG, we recently observed a very similar sustained periodic response elicited by the same type of stimulation (Colon et al., 2016), which was maximal at the scalp vertex and symmetrically distributed over the two hemispheres – a topography that could be explained by activity originating from the left and right operculo-insular cortices (Mouraux et al., 2011). This periodic response was also shown to be predominantly elicited by the activation of heat-sensitive C fiber nociceptors, as it was unaffected by conduction blockade of myelinated A-fibers (Colon et al., 2016). C fiber nociceptors are thought to be the main mediators of primary hyperalgesia induced by tissue injury or inflammation (Campbell and Meyer, 1983; LaMotte et al., 1983). Hence, the proposed approach could allow a better understanding of the involvement of C fibers in physiological and pathological conditions.

However, sustained periodic non-nociceptive vibrotactile stimulation also elicited a sustained periodic insular response at the frequency of

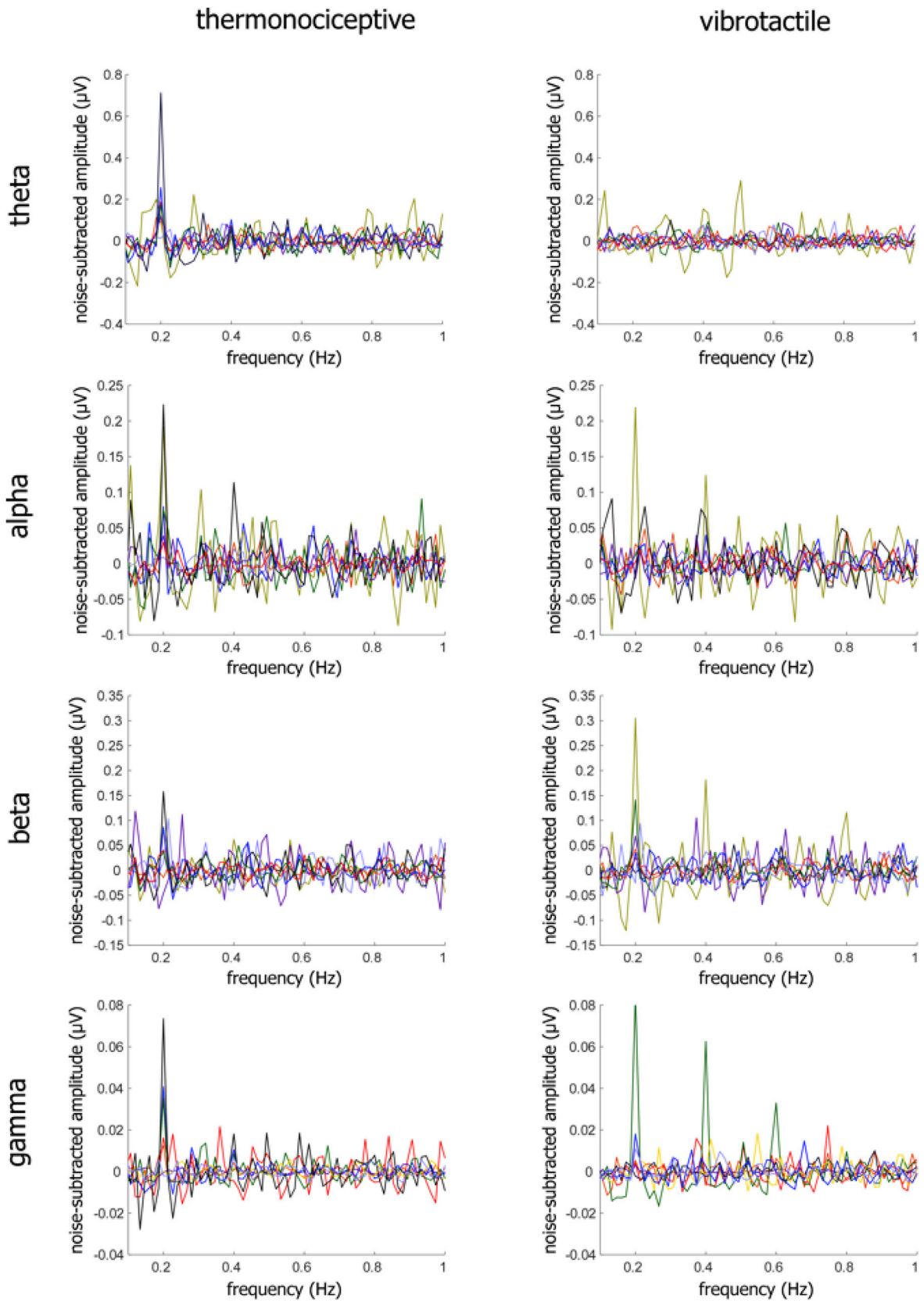

Fig. 7. Periodic modulation of ongoing insular EEG oscillations elicited by sustained 0.2 Hz thermonociceptive and vibrotactile stimulation in the theta, alpha, beta, and gamma frequency bands. Each waveform corresponds to the frequency spectrum of the signal envelope of theta, alpha, beta and gamma-band activity recorded from the insula of one individual participant, at the electrode contact where the signal amplitude was greatest.

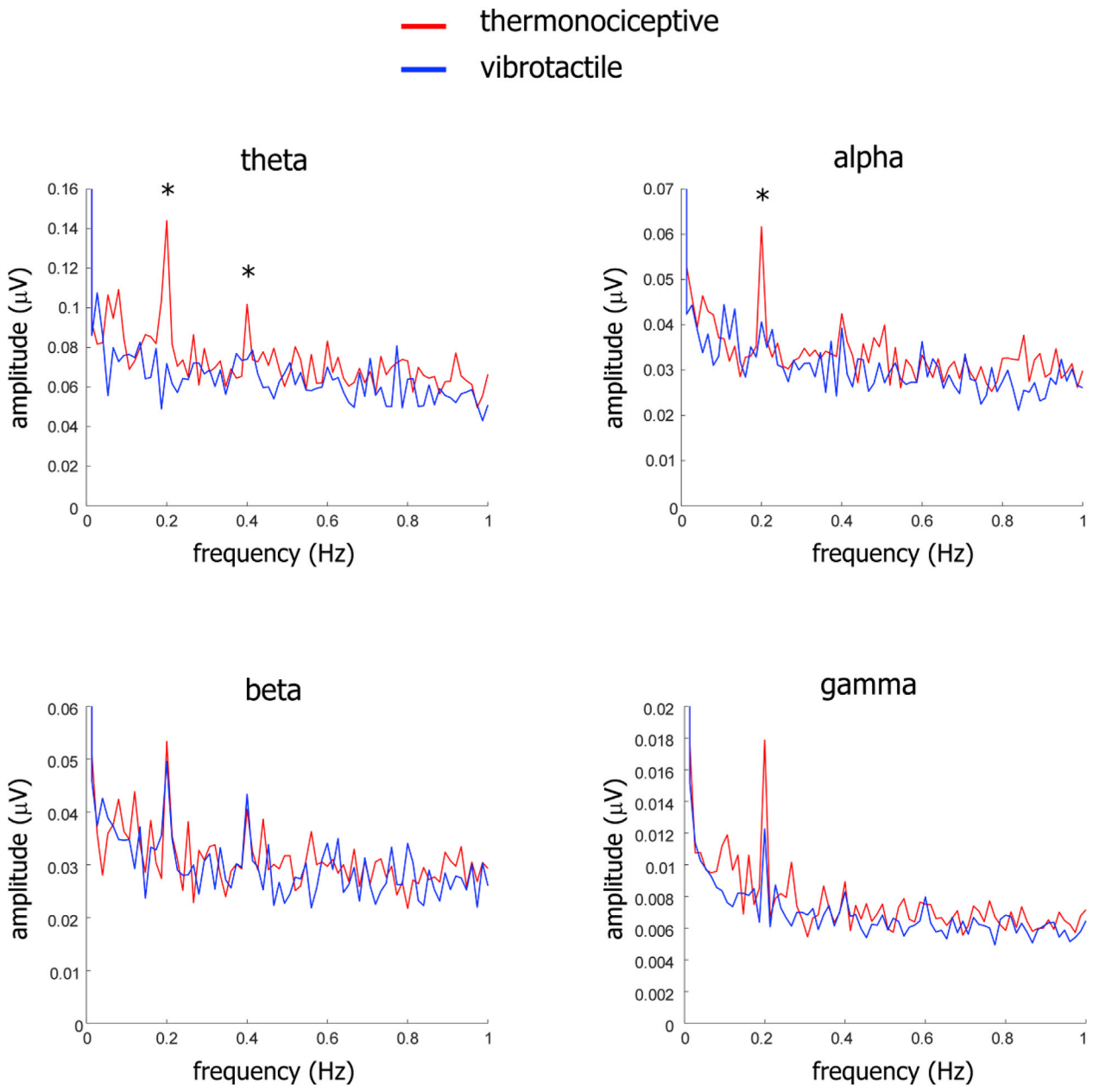

Fig. 8. Group-level average frequency spectrum of the intracerebral EEG signal envelope of theta, alpha, beta, and gamma activity averaged across all insular contacts. Compared to 0.2 Hz vibrotactile stimulation, 0.2 Hz thermonociceptive stimulation elicited a greater modulation of ongoing oscillations at 0.2 Hz and at 0.4 Hz in the theta frequency band (both $p < .001$), and a greater modulation of ongoing oscillations at 0.2 Hz in the alpha frequency band ($p = .002$).

stimulation and at its harmonics. Furthermore, the periodic response elicited by vibrotactile stimulation was indistinguishable from the periodic response elicited by thermonociceptive stimulation – at least at the macroscopic level of intracerebral EEG recordings. First, the two responses did not differ in terms of signal amplitude. Second, they showed a similar spatial distribution, both being markedly more prominent in the posterior insula compared to the anterior insula. Both responses were clearly identifiable in each patient. Differently from transient insular responses evoked by very brief stimuli which were recently shown to be strongly affected by stimulus repetition (Liberati et al., 2018), the sustained periodic responses elicited by thermonociceptive and vibrotactile stimulation maintained their amplitude over time, despite the continuous and long-lasting stimulation. This indicates that the insular responses elicited by sustained periodic somatosensory stimulation and the insular responses elicited by transient somatosensory stimulation reflect functionally distinct processes. Further supporting this functional dissociation is the fact that the insular responses elicited by sustained periodic somatosensory stimulation are maximal at posterior insular contacts, whereas the insular responses elicited by transient somatosensory stimulation are similarly distributed over posterior and anterior insular contacts (Liberati et al., 2017, 2016). Taken together, slow periodic somatosensory stimulation appears to be a robust and reliable method to investigate sustained insular responses to prolonged nociceptive and non-nociceptive somatosensory stimuli.

Compared to single unit recordings, intracerebral EEG recordings performed using macroscopic electrode contacts sample brain activity at population level, and are also more likely to be influenced by distant sources of activity (Herreras, 2016; Kajikawa and Schroeder, 2011). Therefore, one cannot exclude that responses which appear similar when sampled using intracerebral EEG actually reflect the activity of distinct neurons intermingled within the same sub-regions of the insula. Moreover, because each patient generally had a limited number of electrode

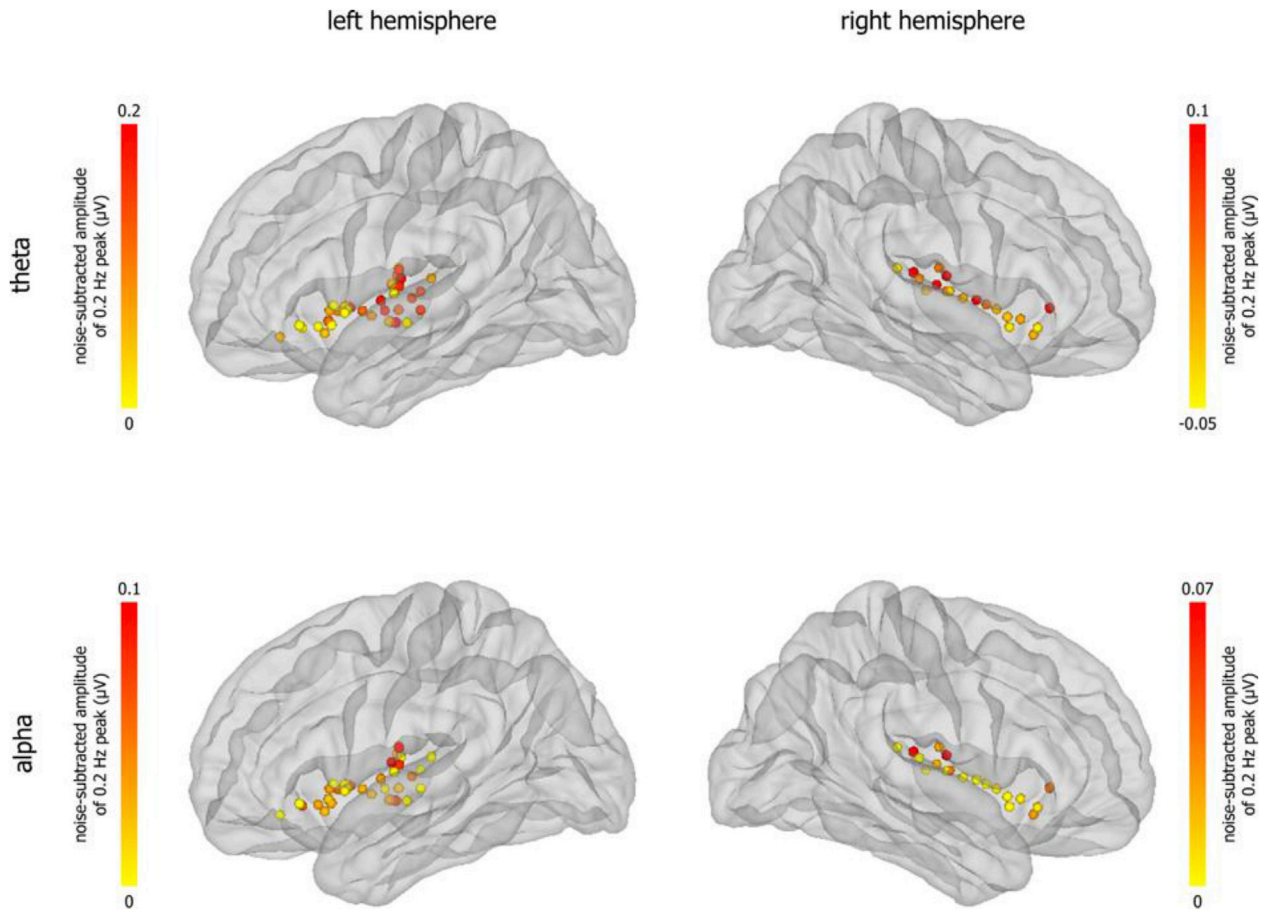

Fig. 9. Spatial distribution of the amplitude of the 0.2 Hz modulation of theta- and alpha-band oscillations induced by sustained 0.2 Hz periodic thermonociceptive stimulation. MNI coordinates of the insular contacts of all patients, within a 3D glass brain generated using the FreeSurfer template (http://surfer.nmr.mgh.harvard.edu/). Both for theta and alpha oscillations, the modulation at 0.2 Hz was greater at dorsal-posterior insular contacts as compared to anterior contacts (theta: $p < .001$; alpha: $p = .019$).

contacts located in a circumscribed sub-region of the insula, one must be cautious when interpreting differences in response amplitude across electrode contacts, as at least part of the observed differences could be due to interindividual differences rather than topographical differences. However, the fact that for both modalities of stimulation the strongest periodic responses were generally recorded from the dorsal posterior regions of the insula suggests that these responses did not originate from distant structures, as activity originating from distant structures would be expected to similarly influence the signals recorded at all insular contacts. Notably, the posterior prominence of the elicited responses is compatible with a preferential involvement of the posterior insula in the processing of somatic input (Baier et al., 2014, 2013; Baumgärtner et al., 2010; Björnsdotter et al., 2009; Bowsher et al., 2004; Brooks et al., 2002; Burton et al., 1995; Greenspan and Winfield, 1992; Hua et al., 2005; Kakigi et al., 2005; Keltner et al., 2006; Kupers and Kehlet, 2006; Schneider et al., 1993; Strigo et al., 2003).

In addition to generating a periodic signal at intracerebral insular contacts, sustained periodic thermonociceptive and vibrotactile stimulation also induced a periodic modulation of ongoing insular oscillations within different frequency bands, also most prominent in the posterior regions of the insula as compared to the anterior regions. Crucially, the periodic modulation of ongoing oscillations induced by periodic thermonociceptive stimulation differed markedly from the periodic modulation of ongoing oscillations induced by periodic vibrotactile stimulation. Indeed, compared to vibrotactile stimulation, thermonociceptive stimulation elicited a markedly stronger modulation of oscillations, at least in theta (4–8 Hz) and alpha (8–12 Hz) frequency bands.

The preferential modulation of alpha-band oscillations exerted by thermonociceptive stimulation is compatible with the results of a number of EEG studies showing that tonic painful stimuli can induce a sustained increase (Le Pera et al., 2000), decrease (Chang et al., 2001a, 2003; Chen and Rappelsberger, 1994; Egsgaard et al., 2009; Ferracuti et al., 1994; Giehl et al., 2014; Huishi Zhang et al., 2016; Nir et al., 2012; Peng et al., 2014; Schulz et al., 2015; Shao et al., 2012), or both decrease and increase (Backonja et al., 1991; Chang et al., 2001b; Dowman et al., 2008) of alpha-band power. This modulation of alpha-band oscillations, which was also evidenced during the expectation of painful stimuli (Babiloni et al., 2005; Franciotti et al., 2009), has been suggested to reflect cortical activation or disinhibition related to the alerting function of pain (Hu et al., 2013; Peng et al., 2014; Peng and Tang, 2016; Pfurtscheller and Lopes da Silva, 1999; Ploner et al., 2006). Similarly to ongoing alpha-band oscillations, ongoing theta-band oscillations were also reported to be modulated by tonic nociceptive stimuli (Chang et al., 2001a, 2002a; Chen et al., 1998; Chen and Rappelsberger, 1994; Chien et al., 2014; Ferracuti et al., 1994; Huber et al., 2006; Huishi Zhang et al., 2016), and alterations in ongoing theta-band oscillations have been reported in a variety of chronic pain patients, including patients with neurogenic pain (Sarnthein et al., 2006; Sarnthein and Jeanmonod, 2008), visceral pain (Drewes et al., 2008), and complex regional pain syndrome (Walton et al., 2010).

A number of studies have also associated tonic pain to the modulation of beta-band (Backonja et al., 1991; Chang et al., 2002a, 2002b; Chen et al., 1989; Chen and Rappelsberger, 1994; Huber et al., 2006; Le Pera et al., 2000; Shao et al., 2012; Veerasarn and Stohler, 1992) and

gamma-band (Dowman et al., 2008; Peng et al., 2014; Schulz et al., 2015; Veerasarn and Stohler, 1992) oscillations. In our study, thermonociceptive stimulation also modulated beta-band oscillations at the frequency of stimulation. In contrast, no significant modulation of beta oscillations was observed during vibrotactile stimuli. However, the magnitude of the modulation induced by thermonociceptive stimulation was not significantly different from the modulation induced by vibrotactile stimulation, suggesting that this feature of insular activity may be non-preferential for thermonociception.

We recently showed that brief thermonociceptive stimuli elicit an early-latency (150–300 ms) enhancement of gamma-band oscillations in the human insula, which appears to be preferential for thermonociception and/or the activation of the spinothalamic system (Liberati et al., 2017). Therefore, it may be surprising that, in the present study, sustained periodic thermonociceptive stimuli did not exert a preferential modulation of ongoing gamma-band oscillations compared to vibrotactile stimuli. Even though the magnitude of gamma-band modulation was not significantly greater for thermonociceptive stimulation as compared to vibrotactile stimulation, the modulation of gamma-band oscillations exerted by periodic thermonociceptive stimulation was significantly greater than zero, whereas the modulation of gamma-band oscillations exerted by vibrotactile stimuli was not. Hence, such as for beta-band oscillations, the absence of a significant difference between the modulation exerted by the two types of stimuli might be explained by limited statistical power. It should be also noted that the brief thermonociceptive stimuli used in our previous study elicited a highly pricking sensation related to the preferential activation of quickly-adapting Aδ fiber nociceptors (Churyukanov et al., 2012), whereas the sustained periodic thermonociceptive stimulation used in the present study elicited a more diffuse burning sensation shown to predominantly relate to the activation of C fibers (Colon et al., 2016). Therefore, the processes underlying the perception of these two types of stimuli are likely very different.

The observation that thermonociceptive stimuli elicit a significant modulation of theta- and alpha-band insular activity whose magnitude is maximal at dorsal posterior contacts is consistent with several fMRI studies showing an increase of BOLD signal in the dorsal posterior insula following nociceptive thermal (Baumgärtner et al., 2010; Brooks et al., 2002; Keltner et al., 2006; Strigo et al., 2003) and mechanical (Baumgärtner et al., 2010; Kupers and Kehlet, 2006) somatosensory stimuli, as well as an increase of absolute cerebral blood flow (CBF) during the perception of tonic heat pain, correlating with subjective reports of pain intensity (Segerdahl et al., 2015b). Moreover, direct electrical stimulation of this region may trigger painful sensations (Mazzola et al., 2012, 2009), and tract tracing and microelectrode studies in primates have suggested its involvement in the cortical processing of incoming nociceptive sensory stimuli (Craig, 2014; Evrard et al., 2014). All these findings support the conclusion that the dorsal posterior insula plays a role in the processing of nociceptive input and/or in pain perception.

Nevertheless, the preferential modulation exerted by sustained periodic thermonociceptive stimuli on ongoing oscillations in the theta and alpha frequency bands recorded from posterior insular contacts should be interpreted with caution. More specifically, it is important to consider that these modulations do not necessarily reflect *pain-specific* insular activity, given that thermonociceptive and vibrotactile stimuli differ in a number of dimensions not restricted to painfulness. For instance, differently from vibrotactile stimuli, thermonociceptive stimuli activate the spinothalamic system and convey thermal information – two characteristics that are not necessarily associated with pain. To disentangle these different properties of thermonociceptive stimulation, further investigations of the modulation of ongoing insular oscillations should be carried out comparing periodic responses to different types of stimuli, such as sustained periodic cool stimuli (which activate the spinothalamic system and convey thermal information, but are not painful), and sustained periodic nociceptive mechanical stimuli (which activate the spinothalamic system, but do not convey thermal information and are not necessarily painful).

In conclusion, both sustained and slow periodic thermonociceptive and vibrotactile stimulation elicit sustained periodic responses in the human insula, particularly in its posterior portion. In addition to this periodic response, thermonociceptive stimulation exerts a preferential modulation of ongoing theta- and alpha-band oscillations, which is not observed in response to vibrotactile stimulation. These results, which are compatible with several findings suggesting a relevant role of the dorsal posterior insula in the processing of nociceptive input, indicate that we can clearly differentiate between insular responses to thermonociceptive and non-nociceptive tactile stimuli by means of a frequency tagging approach. Further investigations using single-unit recordings could shed light on the exact contribution of different neuronal populations to the selective modulation of ongoing theta- and alpha-band oscillations. The identification of oscillatory activities preferential for thermonociception could lead to new insights into the physiological mechanisms of nociception in humans, and offer new prospects for investigating the pathological mechanisms underlying sustained pain.

Data availability

The data used for the manuscript are publicly available from the OSF data repository at the address https://osf.io/zj6rv/files, DOI: https://doi.org/10.17605/OSF.IO/ZJ6RV.

Conflicts of interest

The authors declare no competing financial interests or conflict of interest.

Acknowledgements

A.M., G.L., and M.A. received support from a European Research Council Starting Grant (PROBING-PAIN 336130). G.L. also received support from the Fonds National de la Recherche Scientifique (FNRS, Belgium). The funders had no role in the study design, data collection and analysis, decision to publish, or preparation of the article. The authors declare no competing financial interests. We wish to thank all the members of the Nocions Lab (http://nocions.org) for the useful discussions.

References

Babiloni, C., Brancucci, A., Capotosto, P., Arendt-Nielsen, L., Chen, A.C.N., Rossini, P.M., 2005. Expectancy of pain is influenced by motor preparation: a high-resolution EEG study of cortical alpha rhythms. Behav. Neurosci. 119, 503–511. https://doi.org/10.1037/0735-7044.119.2.503.

Backonja, M., Howland, E.W., Wang, J., Smith, J., Salinsky, M., Cleeland, C.S., 1991. Tonic changes in alpha power during immersion of the hand in cold water. Electroencephalogr. Clin. Neurophysiol. 79, 192–203. https://doi.org/10.1016/0013-4694(91)90137-S.

Baier, B., Zu Eulenburg, P., Best, C., Geber, C., Müller-Forell, W., Birklein, F., Dieterich, M., 2013. Posterior insular cortex - a site of vestibular-somatosensory interaction? Brain Behav 3, 519–524. https://doi.org/10.1002/brb3.155.

Baier, B., zu Eulenburg, P., Geber, C., Rohde, F., Rolke, R., Maihöfner, C., Birklein, F., Dieterich, M., 2014. Insula and sensory insular cortex and somatosensory control in patients with insular stroke. Eur. J. Pain 18, 1385–1393. https://doi.org/10.1002/j.1532-2149.2014.501.x.

Baumgärtner, U., Iannetti, G.D., Zambreanu, L., Stoeter, P., Treede, R.-D., Tracey, I., 2010. Multiple somatotopic representations of heat and mechanical pain in the operculo-insular cortex: a high-resolution fMRI study. J. Neurophysiol. 104, 2863–2872. https://doi.org/10.1152/jn.00253.2010.

Björnsdotter, M., Löken, L., Olausson, H., Vallbo, A., Wessberg, J., 2009. Somatotopic organization of gentle touch processing in the posterior insular cortex. J. Neurosci. 29, 9314–9320. https://doi.org/10.1523/JNEUROSCI.0400-09.2009.

Bowsher, D., Brooks, J., Enevoldson, P., 2004. Central representation of somatic sensations in the parietal operculum (SII) and insula. Eur. Neurol. 52, 211–225. https://doi.org/10.1159/000082038.

Brooks, J.C.W., Nurmikko, T.J., Bimson, W.E., Singh, K.D., Roberts, N., 2002. fMRI of thermal pain: effects of stimulus laterality and attention. Neuroimage 15, 293–301. https://doi.org/10.1006/nimg.2001.0974.

Burton, H., Fabri, M., Alloway, K., 1995. Cortical areas within the lateral sulcus connected to cutaneous representations in areas 3b and 1: a revised interpretation of the second somatosensory area in macaque monkeys. J. Comp. Neurol. 355, 539–562. https://doi.org/10.1002/cne.903550405.

Campbell, J.N., Meyer, R.A., 1983. Sensitization of unmyelinated nociceptive afferents in monkey varies with skin type. J. Neurophysiol. 49, 98–110. https://doi.org/10.1152/jn.1983.49.1.98.

Chang, P.F., Arendt-Nielsen, L., Chen, A.C.N., 2002a. Dynamic changes and spatial correlation of EEG activities during cold pressor test in man. Brain Res. Bull. 57, 667–675. https://doi.org/10.1016/S0361-9230(01)00763-8.

Chang, P.F., Arendt-Nielsen, L., Chen, A.C.N., 2002b. Differential cerebral responses to aversive auditory arousal versus muscle pain: specific EEG patterns are associated with human pain processing. Exp. Brain Res. 147, 387–393. https://doi.org/10.1007/s00221-002-1272-9.

Chang, P.-F., Arendt-Nielsen, L., Graven-Nielsen, T., Chen, A.C.N., 2003. Psychophysical and EEG responses to repeated experimental muscle pain in humans: pain intensity encodes EEG activity. Brain Res. Bull. 59, 533–543.

Chang, P.F., Arendt-Nielsen, L., Graven-Nielsen, T., Svensson, P., Chen, A.C., 2001a. Topographic effects of tonic cutaneous nociceptive stimulation on human electroencephalograph. Neurosci. Lett. 305, 49–52.

Chang, P.F., Arendt-Nielsen, L., Graven-Nielsen, T., Svensson, P., Chen, A.C., 2001b. Different EEG topographic effects of painful and non-painful intramuscular stimulation in man. Exp. Brain Res. 141, 195–203. https://doi.org/10.1007/s002210100864.

Chen, A.C., Dworkin, S.F., Haug, J., Gehrig, J., 1989. Topographic brain measures of human pain and pain responsivity. Pain 37, 129–141. https://doi.org/10.1016/0304-3959(89)90125-5.

Chen, A.C., Rappelsberger, P., 1994. Brain and human pain: topographic EEG amplitude and coherence mapping. Brain Topogr. 7, 129–140. https://doi.org/10.1007/BF01186771.

Chen, A.C., Rappelsberger, P., Filz, O., 1998. Topology of EEG coherence changes may reflect differential neural network activation in cold and pain perception. Brain Topogr. 11, 125–132.

Chien, J.H., Liu, C.C., Kim, J.H., Markman, T.M., Lenz, F.A., 2014. Painful cutaneous laser stimuli induce event-related oscillatory EEG activities that are different from those induced by nonpainful electrical stimuli. J. Neurophysiol. 112, 824–833. https://doi.org/10.1152/jn.00209.2014.

Churyukanov, M., Plaghki, L., Legrain, V., Mouraux, A., 2012. Thermal detection thresholds of Aδ- and C-fibre afferents activated by brief CO2 laser pulses applied onto the human hairy skin. PLoS One 7, e35817. https://doi.org/10.1371/journal.pone.0035817.

Colon, E., Legrain, V., Mouraux, A., 2012a. Steady-state evoked potentials to study the processing of tactile and nociceptive somatosensory input in the human brain. Neurophysiologie Clinique/Clinical Neurophysiology 42, 315–323.

Colon, E., Legrain, V., Mouraux, A., 2014. EEG frequency tagging to dissociate the cortical responses to nociceptive and nonnociceptive stimuli. J. Cognit. Neurosci. 26, 2262–2274. https://doi.org/10.1162/jocn_a_00648.

Colon, E., Liberati, G., Mouraux, A., 2016. EEG frequency tagging using ultra-slow periodic heat stimulation of the skin reveals cortical activity specifically related to C fiber thermonociceptors. Neuroimage 146, 266–274. https://doi.org/10.1016/j.neuroimage.2016.11.045.

Colon, E., Nozaradan, S., Legrain, V., Mouraux, A., 2012b. Steady-state evoked potentials to tag specific components of nociceptive cortical processing. Neuroimage 60, 571–581. https://doi.org/10.1016/j.neuroimage.2011.12.015.

Craig, A.D., 2002. How do you feel? Interoception: the sense of the physiological condition of the body. Nat. Rev. Neurosci. 3, 655–666. https://doi.org/10.1038/nrn894.

Craig, A.D., 2003. Interoception: the sense of the physiological condition of the body. Curr. Opin. Neurobiol. 13, 500–505. https://doi.org/10.1016/S0959-4388(03)00090-4.

Craig, A.D.B., 2014. Topographically organized projection to posterior insular cortex from the posterior portion of the ventral medial nucleus in the long-tailed macaque monkey. J. Comp. Neurol. 522, 36–63. https://doi.org/10.1002/cne.23425.

Davis, K.D., Bushnell, M.C., Iannetti, G.D., St Lawrence, K., Coghill, R., 2015. Evidence against Pain Specificity in the Dorsal Posterior Insula, vol. 4, p. 362. https://doi.org/10.12688/f1000research.6833.1 [version 1; referees: 3 approved]. F1000Res.

Davis, K.D., Kwan, C.L., Crawley, A.P., Mikulis, D.J., 1998. Functional MRI study of thalamic and cortical activations evoked by cutaneous heat, cold, and tactile stimuli. J. Neurophysiol. 80, 1533–1546. https://doi.org/10.1152/jn.1998.80.3.1533.

Dowman, R., Rissacher, D., Schuckers, S., 2008. EEG indices of tonic pain-related activity in the somatosensory cortices. Clin. Neurophysiol. 119, 1201–1212. https://doi.org/10.1016/j.clinph.2008.01.019.

Drewes, A.M., Gratkowski, M., Sami, S.A.K., Dimcevski, G., Funch-Jensen, P., Arendt-Nielsen, L., 2008. Is the pain in chronic pancreatitis of neuropathic origin? Support from EEG studies during experimental pain. World J. Gastroenterol. 14, 4020–4027.

Dubin, A.E., Patapoutian, A., 2010. Nociceptors: the sensors of the pain pathway. J. Clin. Invest. 120, 3760–3772. https://doi.org/10.1172/JCI42843.

Egsgaard, L.L., Wang, L., Arendt-Nielsen, L., 2009. Volunteers with high versus low alpha EEG have different pain-EEG relationship: a human experimental study. Exp. Brain Res. 193, 361–369. https://doi.org/10.1007/s00221-008-1632-1.

Evrard, H.C., Logothetis, N.K., Craig, A.D.B., 2014. Modular architectonic organization of the insula in the macaque monkey. J. Comp. Neurol. 522, 64–97. https://doi.org/10.1002/cne.23436.

Ferracuti, S., Seri, S., Mattia, D., Cruccu, G., 1994. Quantitative EEG modifications during the cold water pressor test: hemispheric and hand differences. Int. J. Psychophysiol. 17, 261–268. https://doi.org/10.1016/0167-8760(94)90068-X.

Franciotti, R., Ciancetta, L., Della Penna, S., Belardinelli, P., Pizzella, V., Romani, G.L., 2009. Modulation of alpha oscillations in insular cortex reflects the threat of painful stimuli. Neuroimage 46, 1082–1090. https://doi.org/10.1016/j.neuroimage.2009.03.034.

Frigo, M., Johnson, S.G., 1998. FFTW: an adaptive software architecture for the FFT. In: Proceedings of the 1998 IEEE International Conference on Acoustics, Speech and Signal Processing, ICASSP '98 (Cat. No.98CH36181). Presented at the 1998 IEEE International Conference on Acoustics, Speech, and Signal Processing. IEEE, pp. 1381–1384. https://doi.org/10.1109/ICASSP.1998.681704.

Frot, M., Faillenot, I., Mauguière, F., 2014. Processing of nociceptive input from posterior to anterior insula in humans. Hum. Brain Mapp. 35, 5486–5499. https://doi.org/10.1002/hbm.22565.

Frot, M., Magnin, M., Mauguière, F., Garcia-Larrea, L., 2007. Human SII and posterior insula differently encode thermal laser stimuli. Cerebr. Cortex 17, 610–620. https://doi.org/10.1093/cercor/bhk007.

Giehl, J., Meyer-Brandis, G., Kunz, M., Lautenbacher, S., 2014. Responses to tonic heat pain in the ongoing EEG under conditions of controlled attention. Somatosens. Mot. Res. 31, 40–48. https://doi.org/10.3109/08990220.2013.837045.

Greenspan, J.D., Winfield, J.A., 1992. Reversible pain and tactile deficits associated with a cerebral tumor compressing the posterior insula and parietal operculum. Pain 50, 29–39.

Groppe, D.M., Bickel, S., Dykstra, A.R., Wang, X., Mégevand, P., Mercier, M.R., Lado, F.A., Mehta, A.D., Honey, C.J., 2017. iELVis: an open source MATLAB toolbox for localizing and visualizing human intracranial electrode data. J. Neurosci. Methods 281, 40–48. https://doi.org/10.1016/j.jneumeth.2017.01.022.

Herreras, O., 2016. Local field potentials: myths and misunderstandings. Front. Neural Circ. 10, 101. https://doi.org/10.3389/fncir.2016.00101.

Herrmann, C.S., 2001. Human EEG responses to 1-100 Hz flicker: resonance phenomena in visual cortex and their potential correlation to cognitive phenomena. Exp. Brain Res. 137, 346–353. https://doi.org/10.1007/s002210100682.

Hu, L., Peng, W., Valentini, E., Zhang, Z., Hu, Y., 2013. Functional features of nociceptive-induced suppression of alpha band electroencephalographic oscillations. J. Pain 14, 89–99. https://doi.org/10.1016/j.jpain.2012.10.008.

Hua, L.H., Strigo, I.A., Baxter, L.C., Johnson, S.C., Craig, A.D.B., 2005. Anteroposterior somatotopy of innocuous cooling activation focus in human dorsal posterior insular cortex. Am. J. Physiol. Regul. Integr. Comp. Physiol. 289, R319–R325. https://doi.org/10.1152/ajpregu.00123.2005.

Huber, M.T., Bartling, J., Pachur, D., Woikowsky-Biedau, S. v, Lautenbacher, S., 2006. EEG responses to tonic heat pain. Exp. Brain Res. 173, 14–24. https://doi.org/10.1007/s00221-006-0366-1.

Huishi Zhang, C., Sohrabpour, A., Lu, Y., He, B., 2016. Spectral and spatial changes of brain rhythmic activity in response to the sustained thermal pain stimulation. Hum. Brain Mapp. 37, 2976–2991. https://doi.org/10.1002/hbm.23220.

Hyvärinen, A., Oja, E., 2000. Independent component analysis: algorithms and applications. Neural Network. 13, 411–430. https://doi.org/10.1016/S0893-6080(00)00026-5.

Kajikawa, Y., Schroeder, C.E., 2011. How local is the local field potential? Neuron 72, 847–858. https://doi.org/10.1016/j.neuron.2011.09.029.

Kakigi, R., Nakata, H., Inui, K., Hiroe, N., Nagata, O., Honda, M., Tanaka, S., Sadato, N., Kawakami, M., 2005. Intracerebral pain processing in a Yoga Master who claims not to feel pain during meditation. Eur. J. Pain 9, 581–589. https://doi.org/10.1016/j.ejpain.2004.12.006.

Keltner, J.R., Furst, A., Fan, C., Redfern, R., Inglis, B., Fields, H.L., 2006. Isolating the modulatory effect of expectation on pain transmission: a functional magnetic resonance imaging study. J. Neurosci. 26, 4437–4443. https://doi.org/10.1523/JNEUROSCI.4463-05.2006.

Kupers, R., Kehlet, H., 2006. Brain imaging of clinical pain states: a critical review and strategies for future studies. Lancet Neurol. 5, 1033–1044. https://doi.org/10.1016/S1474-4422(06)70624-X.

LaMotte, R.H., Thalhammer, J.G., Robinson, C.J., 1983. Peripheral neural correlates of magnitude of cutaneous pain and hyperalgesia: a comparison of neural events in monkey with sensory judgments in human. J. Neurophysiol. 50, 1–26.

Le Pera, D., Svensson, P., Valeriani, M., Watanabe, I., Arendt-Nielsen, L., Chen, A.C., 2000. Long-lasting effect evoked by tonic muscle pain on parietal EEG activity in humans. Clin. Neurophysiol. 111, 2130–2137. https://doi.org/10.1016/S1388-2457(00)00474-0.

Liberati, G., Algoet, M., Klöcker, A., Ferrao Santos, S., Ribeiro-Vaz, J.G., Raftopoulos, C., Mouraux, A., 2018. Habituation of phase-locked local field potentials and gamma-band oscillations recorded from the human insula. Sci. Rep. 8, 8265. https://doi.org/10.1038/s41598-018-26604-0.

Liberati, G., Klöcker, A., Algoet, M., Mulders, D., Maia Safronova, M., Ferrao Santos, S., Ribeiro Vaz, J.-G., Raftopoulos, C., Mouraux, A., 2017. Gamma-band oscillations preferential for nociception can be recorded in the human insula. Cerebr. Cortex 1–15. https://doi.org/10.1093/cercor/bhx237.

Liberati, G., Klöcker, A., Safronova, M.M., Ferrão Santos, S., Ribeiro Vaz, J.-G., Raftopoulos, C., Mouraux, A., 2016. Nociceptive local field potentials recorded from the human insula are not specific for nociception. PLoS Biol. 14 https://doi.org/10.1371/journal.pbio.1002345 e1002345.

Mazzola, L., Isnard, J., Peyron, R., Guénot, M., Mauguière, F., 2009. Somatotopic organization of pain responses to direct electrical stimulation of the human insular cortex. Pain 146, 99–104. https://doi.org/10.1016/j.pain.2009.07.014.

Mazzola, L., Isnard, J., Peyron, R., Mauguière, F., 2012. Stimulation of the human cortex and the experience of pain: Wilder Penfield's observations revisited. Brain 135, 631–640. https://doi.org/10.1093/brain/awr265.

Meyer, R.A., Campbell, J.N., 1981. Myelinated nociceptive afferents account for the hyperalgesia that follows a burn to the hand. Science 213, 1527–1529.

Mouraux, A., Iannetti, G.D., 2008. Across-trial averaging of event-related EEG responses and beyond. Magn. Reson. Imaging 26, 1041–1054. https://doi.org/10.1016/j.mri.2008.01.011.

Mouraux, A., Iannetti, G.D., Colon, E., Nozaradan, S., Legrain, V., Plaghki, L., 2011. Nociceptive steady-state evoked potentials elicited by rapid periodic thermal stimulation of cutaneous nociceptors. J. Neurosci. 31, 6079–6087. https://doi.org/10.1523/JNEUROSCI.3977-10.2011.

Naidich, T.P., Kang, E., Fatterpekar, G.M., Delman, B.N., Gultekin, S.H., Wolfe, D., Ortiz, O., Yousry, I., Weismann, M., Yousry, T.A., 2004. The insula: anatomic study and MR imaging display at 1.5 T. AJNR Am. J. Neuroradiol. 25, 222–232.

Nir, R.-R., Sinai, A., Moont, R., Harari, E., Yarnitsky, D., 2012. Tonic pain and continuous EEG: prediction of subjective pain perception by alpha-1 power during stimulation and at rest. Clin. Neurophysiol. 123, 605–612. https://doi.org/10.1016/j.clinph.2011.08.006.

Nozaradan, S., 2014. Exploring how musical rhythm entrains brain activity with electroencephalogram frequency-tagging. Philos. Trans. R. Soc. Lond. B Biol. Sci. 369, 20130393. https://doi.org/10.1098/rstb.2013.0393.

Nozaradan, S., Mouraux, A., Cousineau, M., 2017. Frequency tagging to track the neural processing of contrast in fast, continuous sound sequences. J. Neurophysiol. 118, 243–253. https://doi.org/10.1152/jn.00971.2016.

Peng, W., Hu, L., Zhang, Z., Hu, Y., 2014. Changes of spontaneous oscillatory activity to tonic heat pain. PLoS One 9, e91052. https://doi.org/10.1371/journal.pone.0091052.

Peng, W., Tang, D., 2016. Pain related cortical oscillations: methodological advances and potential applications. Front. Comput. Neurosci. 10, 9. https://doi.org/10.3389/fncom.2016.00009.

Pfurtscheller, G., Lopes da Silva, F.H., 1999. Event-related EEG/MEG synchronization and desynchronization: basic principles. Clin. Neurophysiol. 110, 1842–1857. https://doi.org/10.1016/S1388-2457(99)00141-8.

Ploner, M., Gross, J., Timmermann, L., Pollok, B., Schnitzler, A., 2006. Pain suppresses spontaneous brain rhythms. Cerebr. Cortex 16, 537–540. https://doi.org/10.1093/cercor/bhj001.

Regan, D., 1989. Human Brain Electrophysiology: Evoked Potentials and Evoked Magnetic Fields in Science and Medicine.

Sarnthein, J., Jeanmonod, D., 2008. High thalamocortical theta coherence in patients with neurogenic pain. Neuroimage 39, 1910–1917. https://doi.org/10.1016/j.neuroimage.2007.10.019.

Sarnthein, J., Stern, J., Aufenberg, C., Rousson, V., Jeanmonod, D., 2006. Increased EEG power and slowed dominant frequency in patients with neurogenic pain. Brain 129, 55–64. https://doi.org/10.1093/brain/awh631.

Schepers, R.J., Ringkamp, M., 2010. Thermoreceptors and thermosensitive afferents. Neurosci. Biobehav. Rev. 34, 177–184. https://doi.org/10.1016/j.neubiorev.2009.10.003.

Schneider, R.J., Friedman, D.P., Mishkin, M., 1993. A modality-specific somatosensory area within the insula of the rhesus monkey. Brain Res. 621, 116–120. https://doi.org/10.1016/0006-8993(93)90305-7.

Schulz, E., May, E.S., Postorino, M., Tiemann, L., Nickel, M.M., Witkovsky, V., Schmidt, P., Gross, J., Ploner, M., 2015. Prefrontal gamma oscillations encode tonic pain in humans. Cerebr. Cortex 25, 4407–4414. https://doi.org/10.1093/cercor/bhv043.

Segerdahl, A.R., Mezue, M., Okell, T.W., Farrar, J.T., Tracey, I., 2015a. The dorsal posterior insula is not an island in pain but subserves a fundamental role - Response to: “Evidence against pain specificity in the dorsal posterior insula” by Davis et al, vol. 4, p. 1207. https://doi.org/10.12688/f1000research.7287.1 [version 1; referees: 2 approved]. F1000Res.

Segerdahl, A.R., Mezue, M., Okell, T.W., Farrar, J.T., Tracey, I., 2015b. The dorsal posterior insula subserves a fundamental role in human pain. Nat. Neurosci. 18, 499–500. https://doi.org/10.1038/nn.3969.

Shao, S., Shen, K., Yu, K., Wilder-Smith, E.P.V., Li, X., 2012. Frequency-domain EEG source analysis for acute tonic cold pain perception. Clin. Neurophysiol. 123, 2042–2049. https://doi.org/10.1016/j.clinph.2012.02.084.

Strigo, I.A., Duncan, G.H., Boivin, M., Bushnell, M.C., 2003. Differentiation of visceral and cutaneous pain in the human brain. J. Neurophysiol. 89, 3294–3303. https://doi.org/10.1152/jn.01048.2002.

Treede, R.D., Meyer, R.A., Raja, S.N., Campbell, J.N., 1995. Evidence for two different heat transduction mechanisms in nociceptive primary afferents innervating monkey skin. J. Physiol. (Lond.) 483 (Pt 3), 747–758.

Twisk, J.W.R., 2005. Applied Multilevel Analysis. A Practical Guide. Cambridge University Press, Cambridge, UK.

Veerasarn, P., Stohler, C.S., 1992. The effect of experimental muscle pain on the background electrical brain activity. Pain 49, 349–360. https://doi.org/10.1016/0304-3959(92)90242-4.

Walton, K.D., Dubois, M., Llinás, R.R., 2010. Abnormal thalamocortical activity in patients with complex regional pain syndrome (CRPS) type I. Pain 150, 41–51. https://doi.org/10.1016/j.pain.2010.02.023.

Wu, J., Ngo, G.H., Greve, D., Li, J., He, T., Fischl, B., Eickhoff, S.B., Yeo, B.T.T., 2018. Accurate nonlinear mapping between MNI volumetric and FreeSurfer surface coordinate systems. BioRxiv. https://doi.org/10.1101/302794.